

PRELIMINARY HIGH-TEMPERATURE OXIDATION DATA IN STEAM-CO₂ IN SUPPORT OF THE ZEST PROCESS

I. G. Wright, B. A. Pint, and Y. Zhang
Oak Ridge National Laboratory

R. A. Bishop, J. C. Farmer, A. F. Jankowski, and R. B. Rebak
Lawrence Livermore National Laboratory

ABSTRACT

Preliminary corrosion measurements have been made on high-temperature alloys exposed in a steam-10% CO₂ mixture intended to simulate the environment produced in a novel combustion process. Exposures were made up to 1000h at 900°C, and 740h at 1135°C at a pressure of 2 MPa. Data were also collected from exposures in ambient pressure air at 900°C to provide a basis for comparison. Representative wrought, high-temperature alloys produced the expected protective external scales in the steam-CO₂ mixture, but also suffered internal penetration, the importance of which increased with temperature. On the basis of a simple linear extrapolation of these limited data, and using an acceptability criterion of less than 100 nm/h (34 mpy) metal loss, only two of the wrought alloys were considered to be acceptable at 900°C, and none at 1135°C. An alumina scale-forming, oxide dispersion-strengthened alloy met the criterion at both temperatures, and aluminized samples of chromia-forming alloys showed good promise.

Keywords: high-temperature alloys; steam-CO₂; high pressure; oxidation kinetics; scale morphologies.

INTRODUCTION

A technology proposed by Clean Energy Systems Inc. (CES) of Sacramento, California—zero emissions steam technology (ZEST)⁽¹⁾—promises to generate electric power from the combustion of a hydrocarbon fuel with oxygen while minimizing the cost of isolating and sequestering the CO₂ produced. Natural gas, or methane which may be derived from coal, is burned in stoichiometric proportions with oxygen to give a two-species gas that comprises approximately 90% H₂O and 10% CO₂ by volume. After expansion through a series of turbines and steam generators or reheaters, the gases are delivered to a condenser where most of the water vapor condenses and the CO₂ separates from the gaseous mixture. The humid CO₂ from the condenser is dewatered, compressed to the required down-hole pressure (approximately 20 MPa) and delivered to a sequestration site such as an injection well. With a maximum rotor inlet temperature (RIT) of 1427°C at a pressure of 2.6 MPa, it is estimated that net plant efficiencies of the order of 55% will be obtainable with essentially total CO₂ sequestration. The energy penalty for this CO₂ separation process is only 3.4%, which is significantly lower than the 20-45% required for other fossil fuel plants⁽¹⁾.

Figure 1a is a schematic diagram of the process, and Fig. 1b shows a detailed schematic diagram of the steam generator. By employing numerous mixing and cool-down sections in the combustor/steam generator, the temperature of the combustion products can be matched to the required inlet temperature of the expansion gas turbines. Nevertheless, some components are likely to be required to operate in a steam-CO₂ gas mixture at high pressures and at temperatures significantly higher than normally encountered. The pressures and temperatures at various locations in Fig. 1 are indicated in Table 1 for three sets of conditions representing current, near-term, and advanced technologies. It is evident that this concept involves some significant materials challenges, since there are few alloys capable of operating at the highest temperatures envisioned, and few if any data on compatibility with steam under these conditions. The present work was initiated to begin generating data on the performance of high-temperature alloys in steam at temperatures representative of their highest service capabilities.

EXPERIMENTAL PROCEDURES

The alloys chosen for study represent the typical classes of high-temperature alloys available for use as tubes and pipes. The compositions are listed in Table 2. No turbine airfoil alloys were included. Alloy samples of thickness 2.8-3.0 mm (except for alloy N07214, which was only available at 0.8 mm) and surface areas of approximately 4 cm² or 28 cm² were obtained from the Metals Samples Company (Munford, Alabama). The large specimens were exposed with a 120 grit surface finish; the smaller specimens were further ground on SiC papers to a 600 grit finish. Additional alumina scale-forming alloys were included in the test at 1135°C. These consisted of alloy PM2000, obtained in the form of bar stock from Metallwerk Plansee, Reutte, Austria, and two model FeCrAlY alloys that were cast and homogenized at 1300°C for 4h at Oak Ridge National Laboratory (ORNL). Specimens approximately 1 mm in thickness and 4 to 6 cm² surface area were cut from these alloys using a diamond saw. In addition, specimens of alloys N12160, N06230, and N06601 were aluminized at ORNL using a CVD process, the details of which are described elsewhere,⁽²⁾ to produce a γ -NiAl outer layer approximately 50 μ m thick, with an underlying interdiffusion zone. These specimens were exposed in the as-aluminized condition. Before exposure, individual specimens were measured to ± 0.01 mm using a digital micrometer, with six separate readings made of the thickness along the center axis of the specimen. This was followed by degreasing in methanol and acetone, and weighing to ± 0.02 mg using a Mettler model AG245 balance. At intervals during the exposures, and after the final exposure, the specimens were reweighed. Finally, the specimens were copper plated to preserve the scale, mounted in epoxy, cross sectioned to allow the thickness to be remeasured, and metallographically polished. Digital images of micrographs were made at appropriate magnifications, and the thickness of sound metal remaining was measured along the length of the specimen centerline as displayed on an LCD computer monitor, using the measuring tool in Adobe Photoshop®. Measurements included the metal thickness lost due to external scale formation and spallation, as well as the maximum penetration of any subscale from the metal surface.

Exposures were made in ambient air at 900°C (single exposure of 500h), and in a steam-10% CO₂ mixture (all gas mixtures are shown as volume percent) at 2 MPa (285 psig) pressure for two 500h cycles at 900, and for a single exposure of 740h at 1135°C. The gas mixture used at 900°C consisted of steam with CO₂ derived from an Ar-25 CO₂ gas mixture (Air Liquide America Corp.); the steam was generated from distilled and deaerated water (0.06-0.08 μ S), which was injected into the gas delivery system at a temperature above its dew point. The resulting environment consisted of 69 steam, 23 Ar, 8 CO₂. In the run at 1135°C, the environment was steam + 10 CO₂, using Air Liquide America Corp.'s ultra-high purity CO₂. The equilibrium oxygen partial pressures in these gases, and 100% steam, at the test temperatures are listed in Table 3.

For the air exposures, single specimens of each alloy were exposed in annealed, lidded alumina crucibles, in laboratory air in a box furnace. Runs were initiated by inserting the loaded crucibles into the cold furnace which was heated to the test temperature over approximately 4 hours. Runs were terminated by turning off the power and furnace cooling. The steam-10 CO₂ exposures were conducted in vertical reaction tubes made of alloy N06230. The specimens were suspended from individual branches of an alumina 'tree' arranged along the centerline of the reaction tube, with each specimen attached to the alumina rod 'branch' by Pt wire. Four specimens of each alloy were exposed in these tests, two each with the small and large surface areas. The overall design and capabilities of the pressurized exposure facility have been described elsewhere⁽³⁾.

Each of the runs in the pressurized rig was started by pressurizing to test pressure of 2 MPa and heating to 150°C below test temperature under Ar (99.999% purity), at which point the reaction gases were admitted, the rig was brought up to the desired temperature, and the gas flow rate was stabilized (approximately 3 cm/min past the specimens). These runs were stopped by switching off the furnace, admitting Ar at pressure, then stopping the reaction gas flow and depressurizing over 2-3h. Typically, the furnace required 18-21h to heat from ambient to test temperature, and 12-14h to cool down. During operation, the steam was condensed upon exiting the rig and the volume of water measured to monitor the steam flow.

RESULTS

Oxidation Kinetics

900°C, Air, Ambient Pressure. Since 900°C is considered to be a high temperature for a number of the alloys tested, an initial exposure in air at ambient pressure was made to provide a basis for comparison of oxidation kinetics and scale morphologies with those formed in steam-CO₂ mixtures. Mass change data following an isothermal exposure of 500h in ambient air at 900°C are shown in Fig. 2a. Except for alloy N12160, all the alloys exhibited minimal scale spallation. Surprisingly, alloys N06601 and S31000 exhibited larger mass gains and metal losses after 500h than did alloy S30403, whereas the good behavior of alloy N06230 was most likely due to decreased scale spallation promoted by its reactive element (La) content. Of the alumina scale-forming alloys, N07214 gained approximately the same mass as the chromia-forming alloy N06230, and twice the mass of alloy 956 and the aluminized alloys because of transient oxidation effects.

The corresponding metal losses determined by metallographic measurements and expressed as linearly-extrapolated rates of annual metal loss, are shown in Fig. 2b, which indicates uniform surface loss + internal penetration. With the exception of alloy N12160, the ranking order was the same as that for the mass change data. Metallographic data are not shown for the aluminized specimens, which were run for a total of 5000h to provide a better indication of scale growth and alloy-coating interdiffusion. Those data have been reported elsewhere⁽⁴⁾. Although it would be reasonable to expect a slower than linear rate of metal loss for alloys that showed little tendency for scale spallation, the linear extrapolation indicated in Fig. 2b was made to suggest rates of annual metal loss that could be compared to established performance criteria. The dashed horizontal line in Fig. 2b represents a criterion from steam boiler practice⁽⁵⁾ for the rate of metal loss that triggers urgent remedial measures; the value is 100 nm/h (or 34 mpy). On this basis, alloys S31000 and N12160 would not be acceptable, and alloys S30403, N06230, and N06601 would be considered marginal for use under these conditions.

900°C, Steam + 10% CO₂, 2 MPa. The oxidation kinetic curves shown in Fig. 3a were based on mass change measurements after two 500h cycles in this test. The data points are from measurements on four specimens of each alloy (two each of surface area 4 and 28 cm²) after 500h, and on two specimens of each alloy after 1000h. The scatter in the data is indicated for some alloys. The curves drawn may not be properly representative of the long-term kinetic behavior, since they were drawn to fit smoothly through only two sets of data points (and zero). Nevertheless, it is evident that severe scale spallation occurred on alloys S30403 and N12160 from the start of the exposure; alloy S31000 also suffered obvious scale loss in the second exposure cycle. Further, the mass loss data will reflect the extent of any metal loss due to evaporation of CrO₂(OH)₂⁽⁶⁾, which may depend on the extent of surface coverage of transient Fe- and Mn-containing oxides, and likely will be different for each alloy. Figs. 3b and c indicate the annual rate of metal loss based on linear extrapolated from metallographic measurements on these specimens. The decrease in rate of metal loss from the 500h to the 1000h test data would be expected assuming that the slower than linear oxidation trends indicated in Fig. 3a were due to diffusion-controlled growth of protective scales. Even so, the 1000h data (Fig. 3c) indicate that alloys S30403, S31000, N12160, and N06601 would fail the 100 nm/h criterion.

Figure 4 provides a comparison of the mass changes from exposures at 900°C of alloy N06230 (nominal chromia-former) and alloy N07214 (alumina-former) in ambient-pressure air; steam-10% CO₂ for 1000h at 2 MPa; and 100% steam for 7000h at 2 MPa using data from earlier, unpublished work⁽⁷⁾. The long-term

performance of aluminized alloy N06230 also is shown. A significant difference is that, for alloy N06230, the rate of mass gain in the first 1000h of exposure was significantly faster in steam-10% CO₂ (and air) than in 100% steam. This is surprising, because:

- (a) higher reactant (steam) pressures typically lead to higher oxidation rates when these are controlled by diffusion processes in the scale;
- (b) the equilibrium oxygen partial pressure in the gas mixture at pressure is some two orders of magnitude lower than in air (Table 3); and
- (c) if there was a significant contribution to metal loss from CrO₂(OH)₂ evaporation⁽⁶⁾, such an effect would have been expected to be similar (or greater) for 100% steam relative to the steam-CO₂ mixture at the same gas flow rate.

For the alumina scale-forming alloy N07214 the rate of mass change in air and in 100% steam initially was rapid, but slowed significantly after approximately 500h, suggesting the eventual formation of a protective scale. The indication from Figs. 3 b and c is that this trend also occurs in the steam-CO₂ environment.

1135°C, Steam + 10% CO₂, 2 MPa. The 300-series iron-based alloys were omitted from this test because they possess neither useful strength nor adequate corrosion resistance under these conditions. Since it is likely that alumina-forming alloys will be required at the higher temperatures, samples of alloy 2000 and experimental FeCrAlYs, along with aluminized versions of alloys N06230, N12160 and N06601, were included. Mass change data after isothermal exposure for 740h are summarized in Fig. 5. Data for duplicate specimens of the uncoated alloys are shown. As in the other tests, uncoated alloy N12160 suffered significant scale spallation. Of the other two chromia-forming alloys, uncoated specimens of alloy N06230 exhibited mass gains that were very similar to those projected for the same time at 900°C, suggesting an increased contribution to mass loss from scale volatilization. In contrast, the mass gains for alloy N06601 were up to twice those projected for the same time at 900°C, due to increased internal attack (detailed in the following section). As expected, the alumina-forming alloys exhibited much smaller mass gains; the scale spallation observed from one of the alloy N07214 specimens, and from the aluminized specimens of alloys N06230 and N06601, probably represented loss of transient oxides that typically form on such surfaces⁽⁸⁾. The extensive internal oxidation experienced by alloy N07214 in these tests typically has not been observed in air exposures to 10 kh at 1100°C⁽⁹⁾.

Linearly-extrapolated corrosion rates from metallographic measurements for all the wrought, non-aluminized specimens exposed shown in Fig. 5b, suggest that, with the exception of alloy 956 (and one specimen of alloy N06230), the alloys would fail the criterion of 100 nm/h metal loss.

Scale Morphologies

Alloy S30403 formed a thin, uniformly-thick protective scale after 500h in air at 900°C (Fig. 6a); the only internal attack observed consisted of occasional penetration of oxide down alloy grain boundaries that intersected the surface. This alloy was attacked at a significantly faster rate in the steam-CO₂ mixture at 900°C and 2 MPa, forming scales that were voluminous and iron-rich with bright-appearing, fine metallic particles that appeared to delineate different layers of scale. After 500h there were approximately 15 such layers across the thickness of the retained scale, with the nominal thickness of the layers decreasing inward from the scale-gas interface (Fig. 6b). There was also obvious penetration of oxide along the alloy grain boundaries at the reaction front. Obvious separations in the scale parallel to the metal-oxide interface indicated that massive scale spallation was very likely after extended exposures. Equilibrium calculations indicated that the reaction products expected on 304L in air are oxides M₂O₃ and M₃O₄ in the ratio 89:10, whereas in the steam-CO₂ mixture 96 percent of the scale is expected to be M₃O₄. The predominance of M₃O₄ in the faster-growing scale also is consistent with observations of austenitic stainless steels in air-water vapor mixtures^(6,10).

After 1000h in the steam-CO₂ mixture, significant scale loss had occurred from the cooled specimen. The scale had the same appearance as after 500h but was much thicker, and exhibited essentially the same number of bright particle-delineated layers. Alloy grain boundary penetration was deeper than after 500h (Fig. 6c).

Alloy S31000 formed similar-appearing scales in air as in the steam-CO₂ mixture at 900°C and 2 MPa. In air the scale was mostly thin and relatively uniform in thickness, with occasional areas where an outer layer of transient oxide was present (Fig. 7a). The metal-oxide interface consisted of numerous small intrusions into the base metal with occasional deeper penetration down alloy grain boundaries. No breakaway behavior was observed on alloy S31000 in the steam-CO₂ mixture. The scale had the same morphology as in air but was significantly thicker (Fig. 7b). The outer oxide layer formed in the steam-CO₂ environment was more continuous, and appeared to be relatively porous. Penetrations down alloy grain boundaries were deeper and became more numerous after 1000h (Fig. 7c). Fine internal oxide precipitates were present to a depth similar to the maximum grain boundary penetration in air. The thermodynamically-expected equilibrium scales for this alloy were 65:32 M₂O₃:M₃O₄ in air, with 95 percent of the scale being M₃O₄ in the steam-CO₂ mixture--a much less drastic change than for S30403.

Alloy N06230 formed relatively thin, uniform scales in air at 900°C. Those formed in the steam-CO₂ mixture at 900, and at 1135°C and 2 MPa were thinner than in air, presumably as a result of Cr volatilization losses. In all cases, there was occasional deep penetration of oxide along alloy surface grain boundaries (Fig. 8). In some areas the scale formed in the steam-CO₂ mixture was locally thickened to form small nodules. A further difference compared to air exposure was the appearance of a zone of internal oxide precipitates immediately beneath the main scale. These became smaller, but penetrated deeper at 1135°C (Fig. 8d).

Alloy N06601. The external scale formed on this alloy was very similar in appearance to that on alloy N06230, but was thicker under all conditions (Fig. 9). The population, size, and depth of the band of discrete internal oxide precipitates was similar in both atmospheres at 900°C, and increased with time and temperature. Essentially all of the alloy surface grain boundaries contained continuous oxide penetrations which were deeper after exposure in air at 900°C than in the steam-CO₂ mixture, and which accounted for the greater loss of sound metal thickness compared to alloy N06230. The internal oxides were predominantly Al-rich, indicating that the Al content of the alloy (1.4 wt%) is insufficient to form a continuous protective layer. Although higher alloy interdiffusion rates prevail at 1135°C, the more extensive subscale suggests the possibility of enhanced oxygen solubility and/or transport into the alloy in the steam-CO₂ gas mixture.

Alloy N12160 suffered severe scale spallation under all test conditions. In both environments, most of the scale had spalled with separation occurring along the scale-metal interface; the scale remaining in place after 500h at 900°C consisted of a relatively uniform layer of Cr-rich oxide, with a subscale of discrete, Si-rich internal oxide particles and deeper individual penetrations along alloy grain boundaries. Some surface grains become completely surrounded (Figs. 10a, b). In some areas an outer layer of external scale was present that exhibited distinct crystallographic features. After 1000h at 900°C in the steam-CO₂ mixture, the remaining scale consisted of a thin, apparently continuous Si-rich oxide layer which was contiguous with the subscale, with only traces of an outer Cr-rich layer (Fig. 10c). Further, there were significantly fewer discrete subscale particles. After 740h at 1135°C, very little scale remained on the alloy surface after cooling from test temperature. The few areas of remaining scale are typified by that shown in Fig. 10d, and consisted of a thin layer of an apparently two-phase scale, the inner part of which had the appearance of discrete, semi-circular zones with small fingers penetrating into the alloy. Subscale penetration was significantly increased compared to that at 900°C.

Alloy N07214 is expected to form a protective scale based on alumina, capable of providing superior protection to the chromia-rich scale formed by alloys such as alloy N06230. The scales formed in these tests were, in general, thin and apparently adherent (Fig. 11). Although there were areas of local thickening, there were no features obvious in optical metallography that indicated significant differences in the scale formed in any of the tests. However, under all of the test conditions the mass change and loss of sound metal values were very similar to those of alloy N06230, presumably because of the relatively rapid external oxidation experienced by alloy N07214 during the prolonged transient oxidation period (compared to the total exposure times). This is apparent from Fig. 4b, which illustrates the relatively large initial mass gain due to the formation of transient, Ni-rich oxides, with a transition to a much lower oxidation rate after approximately 1000h at 900°C in 2 MPa steam when a continuous layer of alpha alumina forms. The relatively high value for the loss of sound metal was caused

by deep oxide penetrations along many of the alloy surface grain boundaries; as mentioned earlier, this form of attack has not been observed in air.

Alloy 956 formed a thin scale, mostly of uniform thickness, with occasional small areas that were typically twice the nominal thickness. The outer surfaces of the scale formed at 900°C in air exhibited needle- or plate-like features (probably of $\text{-Al}_2\text{O}_3$) of lengths up to 50% of the thickness of the dense scale (Fig. 12a). After 500h at 900°C in the steam-CO₂ mixture the scale was significantly thinner than in air, and the population and length of the external needle/plate features were much reduced (Fig. 12b). After 1000h at 900°C and 740h at 1135°C in the steam-CO₂ mixture the scales were thicker, as expected, and essentially devoid of any outer needle/plate features (Figs. 12c,d). No internal penetration was observed in this alloy; the penetration values indicated in the kinetic diagrams represent incidences of local thickening of the external scale.

DISCUSSION

For alloy S30403 stainless steel, the steam-CO₂ mixture was significantly more aggressive than air at 900°C, such that the alloy experienced breakaway oxidation in the first 500h of exposure. The scales formed (Fig. 6b,c) were very similar to those formed after breakaway in humid air (10% water vapor)⁽⁹⁾, in stark contrast to the protective behavior shown after 500h in air (Fig. 6a). Alloy S31000 exhibited more extensive internal penetration in air than did alloy S30403. The reversal of rankings of these two alloys in the steam-CO₂ mixture resulted from the ability of S31000 with its higher Cr content to form protective scales similar to those formed in air.

While the Ni-Cr alloys--N06230, N06601, and N12160--formed continuous, protective scales under all test conditions, a major factor discriminating their performance was the extent of sound metal loss by internal penetration. However, it should be noted that the metallographic data reported represent the maximum, not average, values measured for uniform metal loss and internal penetration, on the premise that failure initiates at the point of minimum remaining sound metal thickness. A possible objection to this approach is that a single deep internal penetration, which could possibly be a 'rogue' event, can dominate the metal loss values as reported here.

The general form of the internal penetration was similar in both environments at 900°C, but there appeared to be a trend to more numerous small protrusions from the inner part of the external scale and an increased population of fine internal precipitates in the steam-CO₂ mixture. These features were more prevalent after 1000h at 900°C, and at 1135°C. The extent of such internal penetration resulted in the failure of alloy N06601 to meet the acceptability criterion in either gas; this was a surprise, since alloy N06601 is generally considered to be one of the more oxidation-resistant alloys in this class because of its ability to form a protective alumina subscale⁽¹¹⁾. The main external scale formed on alloy N12160 was particularly prone to spallation, as a result of which this alloy showed the highest mass gain after 500h in air; it also had a higher mass loss than the other high-Cr alloys in the steam-CO₂ mixture at 900 and 1135°C. In addition, this alloy exhibited the greatest depth of internal penetration of all the high-temperature alloys under all test conditions. The internal precipitates in alloy N12160 contained Si; after 1000h at 900°C and 740h at 1135°C, the discrete precipitates largely had been replaced by a thin, continuous, Si-containing scale that remained on the surface after cooling from test.

In steam-containing environments at high temperatures, the possibility of the formation of volatile oxy-hydroxide species of Cr⁽⁶⁾ (Si and Al also form volatile oxy-hydroxides, but their contribution is small at 900°C) suggests that material loss by vaporization will occur where the gas contacts Cr-rich metal or oxide surfaces. While no provision was made consistently to determine the extent of such losses in these tests, if present they would have been included in the metallographic measurements of uniform metal loss; also, there was some suggestion of void formation in the alloys N06230 and N06601 in the steam-CO₂ mixture (but not in air), that may signal loss of Cr by this route. Alloys that contain sufficient Mn may be less susceptible to evaporative loss through the formation of an external layer of Mn-rich spinel,⁽¹²⁾ but this may only have been applicable to alloy S31000 in these tests. Detailed concentration profiles in the surfaces of these specimens had not been made to quantify this effect at the time of publication.

The alumina-forming alloys N07214 and 956, as well as the aluminized specimens exhibited the expected protective behavior in both environments. At 900°C, there appeared to be a prolonged period of transient oxidation accompanied by the formation of a subscale until the desired alumina scale was formed on alloy N07214, which probably explains its relatively large mass gains in the 500h exposures compared to alloy 956.

SUMMARY AND CONCLUSIONS

These preliminary, short-term results suggest that, with the exception of alloy S30403 stainless steel, the rate of metal loss at 900°C of typical chromia- and alumina-forming alloys in a steam-10%CO₂ mixture at 2 MPa is of the same order as that in air at ambient pressure. However, the rate of attack in both environments is significant. Comparison with results from similar exposures in steam alone indicates that the attack of chromia-forming alloy N06230 is more aggressive in the steam-CO₂ mixture (and in air) than in steam alone, whereas the corrosion rate for the alumina-forming alloy N07214 appears similar in all three environments. If a criterion for an acceptable rate of metal loss of less than 100 nm/h is used, a conservative, linear extrapolation of the data shows that of the alloys tested that rely on the formation of a chromia-based protective scale, only alloy N06230 would be considered to provide acceptable service in the steam-10%CO₂ mixture at 2 MPa and 900°C, and none would be acceptable at 1135°C. Both alumina-forming alloys, N07214 and 956, would be considered acceptable for service at 900°C, but only alloy 956 at 1135°C. Since the conclusions presented here are based on few data points and relatively short exposures, and since internal penetration was a major contributor to the reported loss of sound metal, it is quite possible that longer-term data will indicate that the linear extrapolation used is too conservative. If this is the case, the range of application of conventional, wrought high-temperature alloys will be wider than suggested here.

Clearly, the choice of available materials suitable for use in the steam-10%CO₂ environment produced in the combustion system proposed in Clean Energy Systems' ZEST process⁽¹⁾ becomes very limited as the temperature is increased to 1135°C. The effect on corrosion behavior of higher pressures is not known, and cannot be predicted with any certainty until it is known whether or not there is a change in the dominant corrosion mechanism, which depends on the relative contributions of cation and anion transport to oxide growth, and the relative importance of the formation and loss of volatile species. Air oxidation data⁽⁹⁾ suggest that alumina-forming alloys (and coatings) may provide acceptable performance up to 1200-1250°C, but experience in the fabrication, use, and repair of alumina-forming alloys applied in high-temperature processes is extremely limited. Further, the effectiveness of alumina-forming coatings is highly dependent on their interaction with the coated substrate, for which few data are available for typical wrought, high-temperature alloys. Possibly, experience with such coatings on aircraft gas turbine alloys could provide some guidelines for their likely behavior, though the available data probably are relatively short-term compared to the needs of land-based power generation applications. Since none of the available alloys will have sufficient useable strength at the higher temperatures of interest, there may be some merit in exploring the application of cooling along with thermal barrier coatings to these alloys⁽¹³⁾.

ACKNOWLEDGEMENTS

The data presented were compiled from results from research supported by the University of California, Lawrence Livermore National Laboratory, contract No. B522650, and the Fossil Energy Advanced Research Materials (ARM) Program, U.S. Department of Energy, under contract DE-AC05-96OR22464 with UT-Battelle LLC. The authors would like to acknowledge the contributions of the following staff members at ORNL: K. M. Cooley and Y. Zhang prepared the aluminized coatings; the experimental exposures were performed by K. S. Reeves and G. W. Garner; H. F. Longmire was responsible for the metallographic preparation of the samples. Finally, we would like to thank P. F. Tortorelli and S. J. Pawel for reviewing the manuscript.

REFERENCES

1. See, for instance, R. Anderson, H. Brandt, S. Doyle, K. Pronske F. Viteri, "Power Generation with 100%

- Carbon Capture and Sequestration,” Presented at the *2nd Annual Conference on Carbon Sequestration*, Alexandria, VA, May 5-8, 2003.
2. W.Y. Lee, Y. Zhang, I.G. Wright, B.A. Pint, and P.K. Liao, *Met. Trans*, 29A, 833 (1998).
 3. J.R. Keiser, M. Howell, J.J. Williams, and R.A. Rosenberg, “Compatibility of Selected Ceramics with Steam-Methane Reformer Environments,” Paper 140 in *Corrosion/96*, NACE International (1996).
 4. B.A. Pint, Y. Zhang, J.A. Haynes, and I.G. Wright, *Proc. 17th Annual Conference on Fossil Energy Materials*, Baltimore, Maryland, April 22-24, 2003; see ‘Conference Proceedings’ at <http://www.netl.doe.gov/>
 5. Criterion used by the Central Electricity Generating Board, UK, as a decision point for increased surveillance, and possible repair or replacement, of steam generator tubes in coal-fired boilers.
 6. H. Asteman, J.-E. Svensson, L.-G. Johansson and M. Norell, “Indication of Chromium Oxide Hydroxide Evaporation During Oxidation of S30403 at 873K in the Presence of 10% Water Vapor,” *Oxidation of Metals*, 52, 95-111 (1999).
 7. I.G. Wright and B.A. Pint, Oak Ridge National Laboratory, unpublished work, 2002.
 8. B.A. Pint, K.L. More and I.G. Wright, “The Use of Two Reactive Elements to Optimize Oxidation Performance of Alumina-Forming Alloys,” *Materials at High Temperature*, in press (2003).
 9. B.A. Pint, P.F. Tortorelli and I.G. Wright, “Effect of Cycle Frequency on High Temperature Oxidation Behavior of Alumina-Forming Alloys,” *Oxidation of Metals*, 58, 73-101 (2002).
 10. B.A. Pint, R. Peraldi, and P.F. Tortorelli, NACE paper 03-499, Houston, Texas, March 2003.
 11. See, for instance, Inconel N06601 Data Sheet, Metal Technology, Inc., Albany, Oregon, USA.
 12. W.J. Quadackers, T. Malkow, J. Piron-Abellan, U. Flesch, V. Shemet, and L. Singheiser, pp. 827-836 in Vol. 2 of *Proc. 4th European Fuel Cell Forum*, J. McEvoy, Ed., Elsevier, Amsterdam, The Netherlands (2000).
 13. B.A. Pint, I.G. Wright, and W.J. Brindley, “Evaluation of TBC Systems on Novel Substrates,” *J. Therm. Spray Techn.*, 2 (2), 198-203 (2000).

TABLE 1
TURBINE OPERATING CONDITIONS FOR THE ZEST PROCESS

Turbine Inlet Conditions	Current Technology		Near-Term Technology		Advanced Technology	
	°C	MPa	°C	MPa	°C	MPa
High-pressure turbine	649	14.83	816	14.83	983	14.83
Intermediate-pressure turbine	566	2.62	1205	2.62	1427	2.62
Low-pressure turbine	566	0.12	649	0.12	816	0.12
Plant efficiency*	40		46		55	

*based on the lower heating value of the coal used to make syngas; assumes no syngas plant losses.

TABLE 2
CHEMICAL COMPOSITIONS OF ALLOYS TESTED (wt%)

Alloy/UNS	Heat No.	Fe	Ni	Co	W	Cr	Al	Mo	Si	Mn	C	S ^a
S30403	YK98	Bal	8.55			18.13		0.35	0.31	1.71	0.016	50
S31000	AL871799	Bal	19.37			25.45		0.4	0.63	1.63	0.04	4
N06230		1.54	Bal	0.17	14.23	22.45	0.34	1.42	0.38	0.52	0.10	20
N06601	AL510348	14.8	Bal			22.52	1.37		0.37	0.33	0.03	2
N12160	872717163	0.1	Bal	30.5		27.8	0.05	0.35	2.57	0.43	0.05	20
N07214		3.52	Bal		0.1	16.34	4.43	0.1	0.1	0.2	0.04	20
Inconel MA956 ^d	JBD0201	Bal	0.11	0.03		19.01	4.87		0.05	0.12	0.01	70
PM2000		Bal	0.02	0.02		20.13	5.54		0.02	0.04	0.01	31
FeCrAlY ^e		Bal				20.07	5.08				<0.01	10
FeCrAlY+Hf ^f		Bal	0.01			20.21	5.22				<0.01	10

a: ppmw

d: also 0.49 Y₂O₃

b: also 0.02La

e: also 0.14Y

c: also 0.08Y; 0.03Zr

f: also 0.06Hf, 0.004Y

TABLE 3
EQUILIBRIUM OXYGEN PARTIAL PRESSURES (atm)

Gas	Ambient		2 MPa	
	900°C	1135°C	900°C	1135°C
Air	1.9 x 10 ⁻¹	1.9 x 10 ⁻¹	3.43	3.42
Steam	2.33 x 10 ⁻⁶	4.00 x 10 ⁻⁵	1.52 x 10 ⁻⁵	2.61 x 10 ⁻⁴
Steam-10%CO ₂	2.37 x 10 ⁻⁶	4.31 x 10 ⁻⁵	1.55 x 10 ⁻⁵	2.81 x 10 ⁻⁴

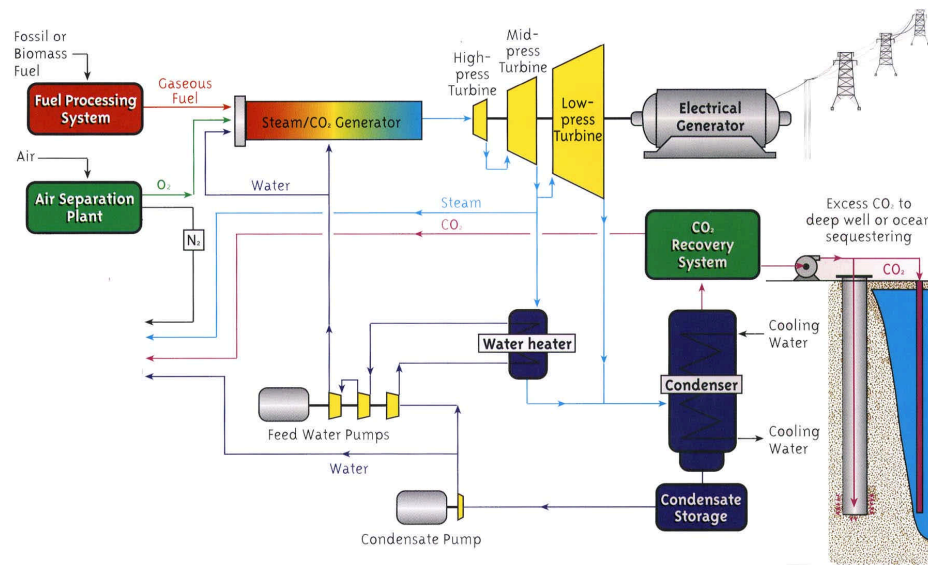


FIGURE 1a - Schematic diagram of the process

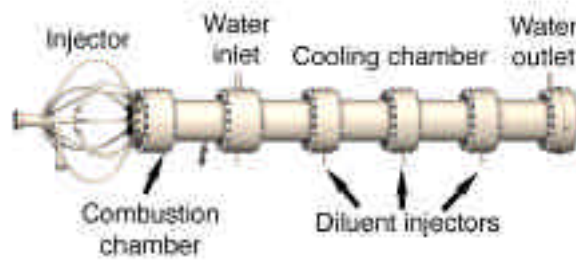
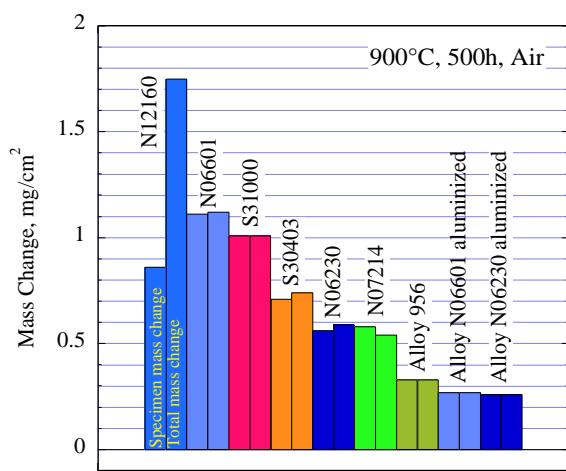
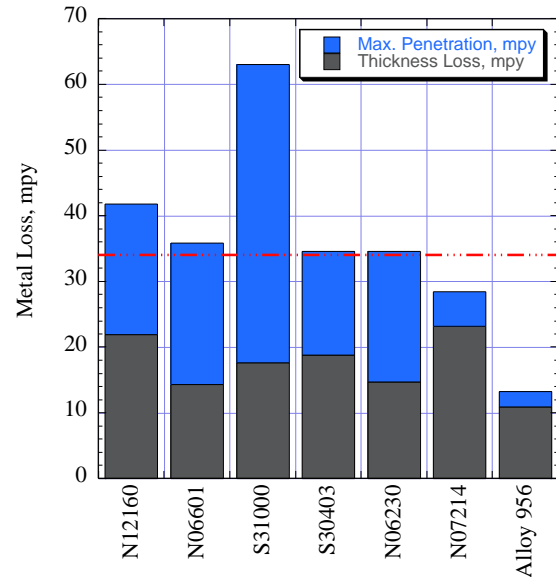


FIGURE 1b - Detail of the gas generator

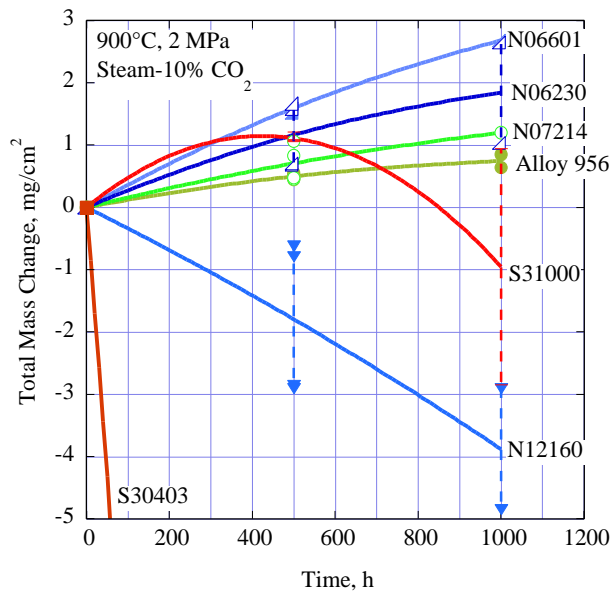


(a)

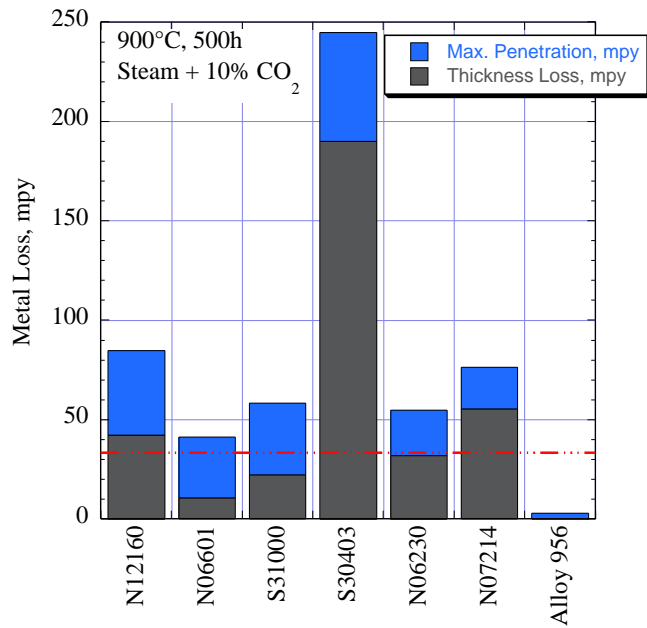


(b)

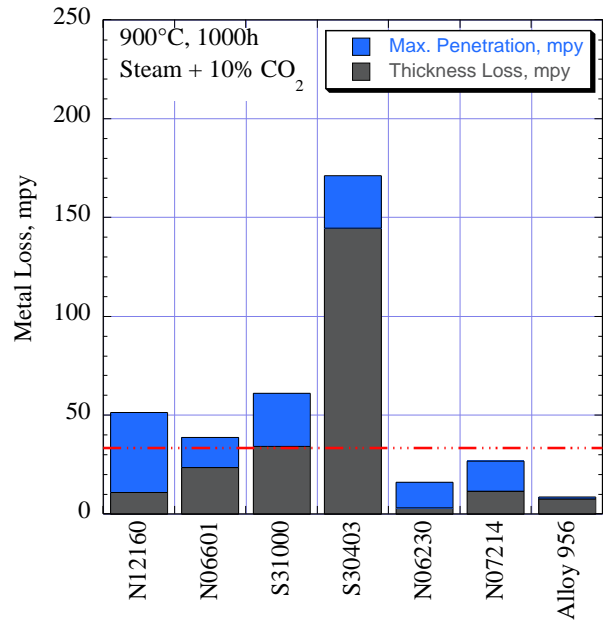
FIGURE 2 - Corrosion after isothermal exposure for 500h to ambient air at 900°C (a) mass gains: for each alloy, the first column represents the mass change of the specimen, the second the total mass gain (specimen + spallation products); the difference is an indication of the severity of scale spallation; (b) corrosion rates linearly-extrapolated from optical measurements of metal loss, defined as uniform thickness loss + internal penetration.



(a)



(b)



(c)

FIGURE 3 - Oxidation kinetics from exposure at 900°C to a steam + 10% CO₂ mixture at 2 MPa pressure. The exposure consisted of 2 x 500h cycles. In (b) and (c), corrosion rates were derived for comparison purpose only based on a linear extrapolation of the 500h and after 1000h data.

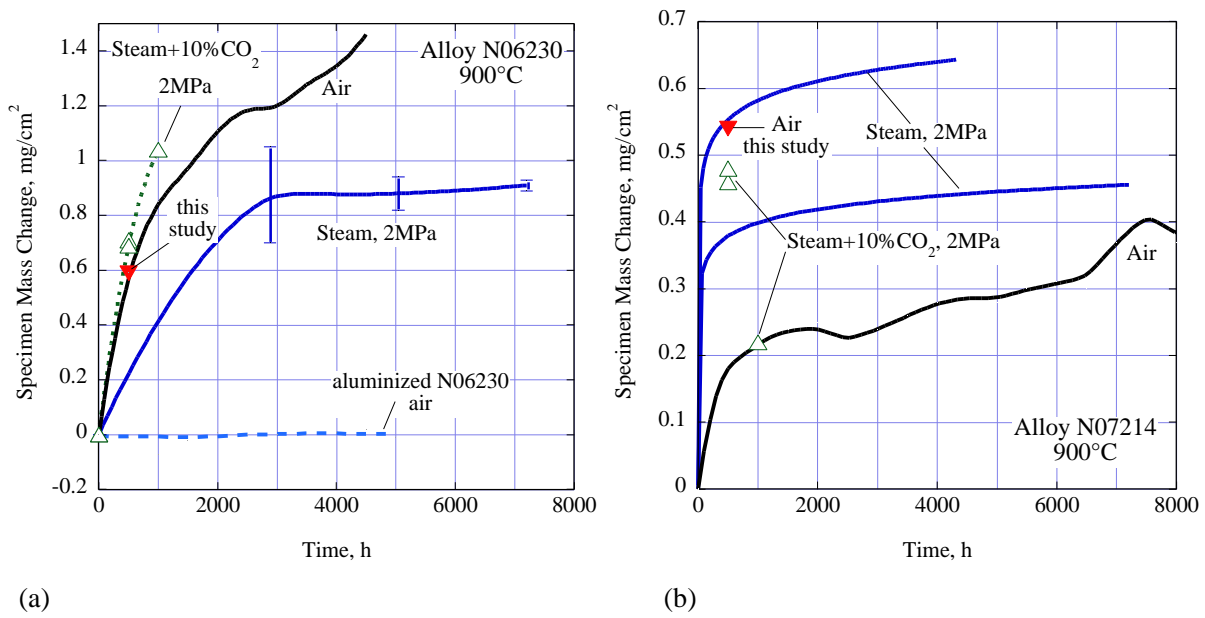


FIGURE 4 - Comparison of mass changes of (a) alloy N06230, and (b) alloy N07214 after exposure at 900°C in air, and in steam + 10% CO₂ at 2 MPa, with those in steam at 2 MPa. Note the difference in specimen mass change scales. Steam data from unpublished earlier work.⁽⁷⁾

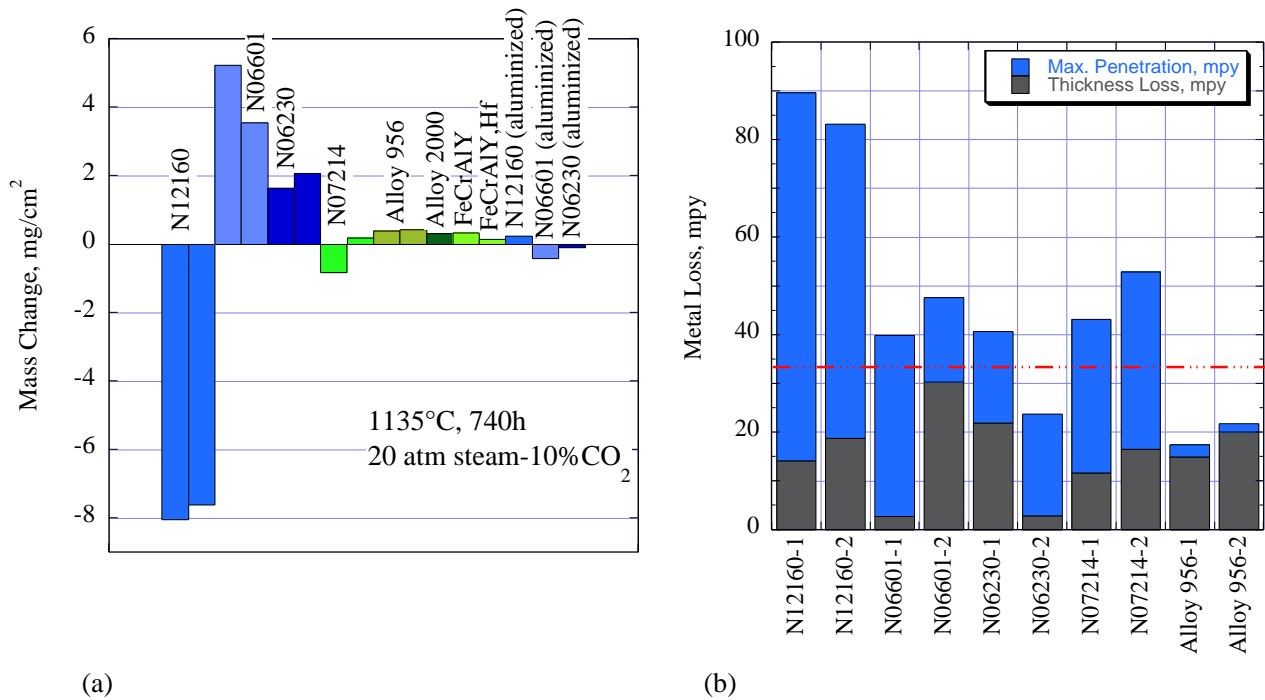


FIGURE 5 – Kinetic data for alloys exposed isothermally for 740h exposure at 1135°C to a steam + 10% CO₂ mixture at 2 MPa pressure (a) mass change data; (b) metallographic measurements (corrosion rates derived for comparison purposes only).

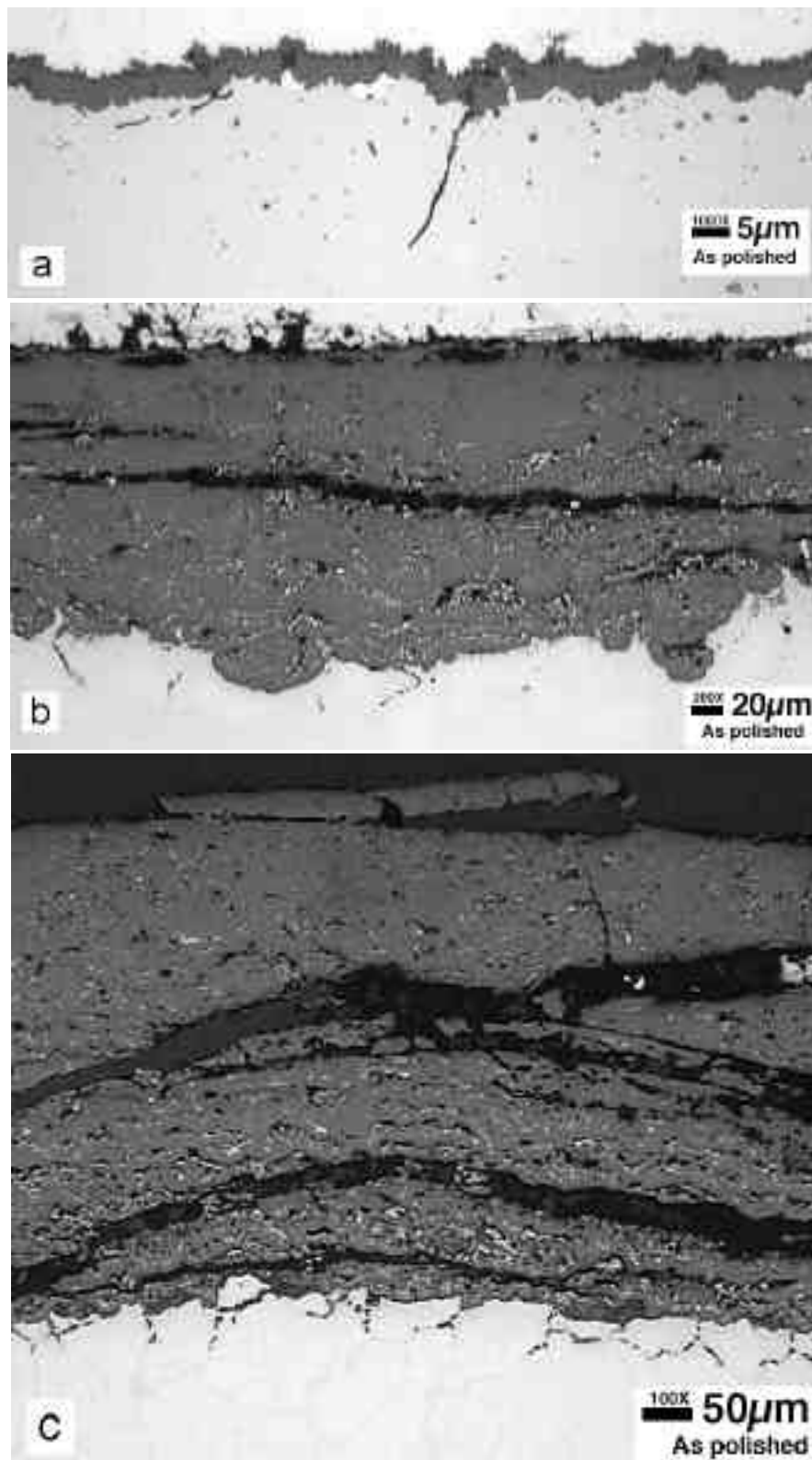


FIGURE 6 - Metallographic cross sections of alloy S30403 stainless steel after exposure in (a) air at 900°C for 500h; and (b and c) steam-10%CO₂ at 2 MPa and 900°C for 500h and 1000h, respectively.

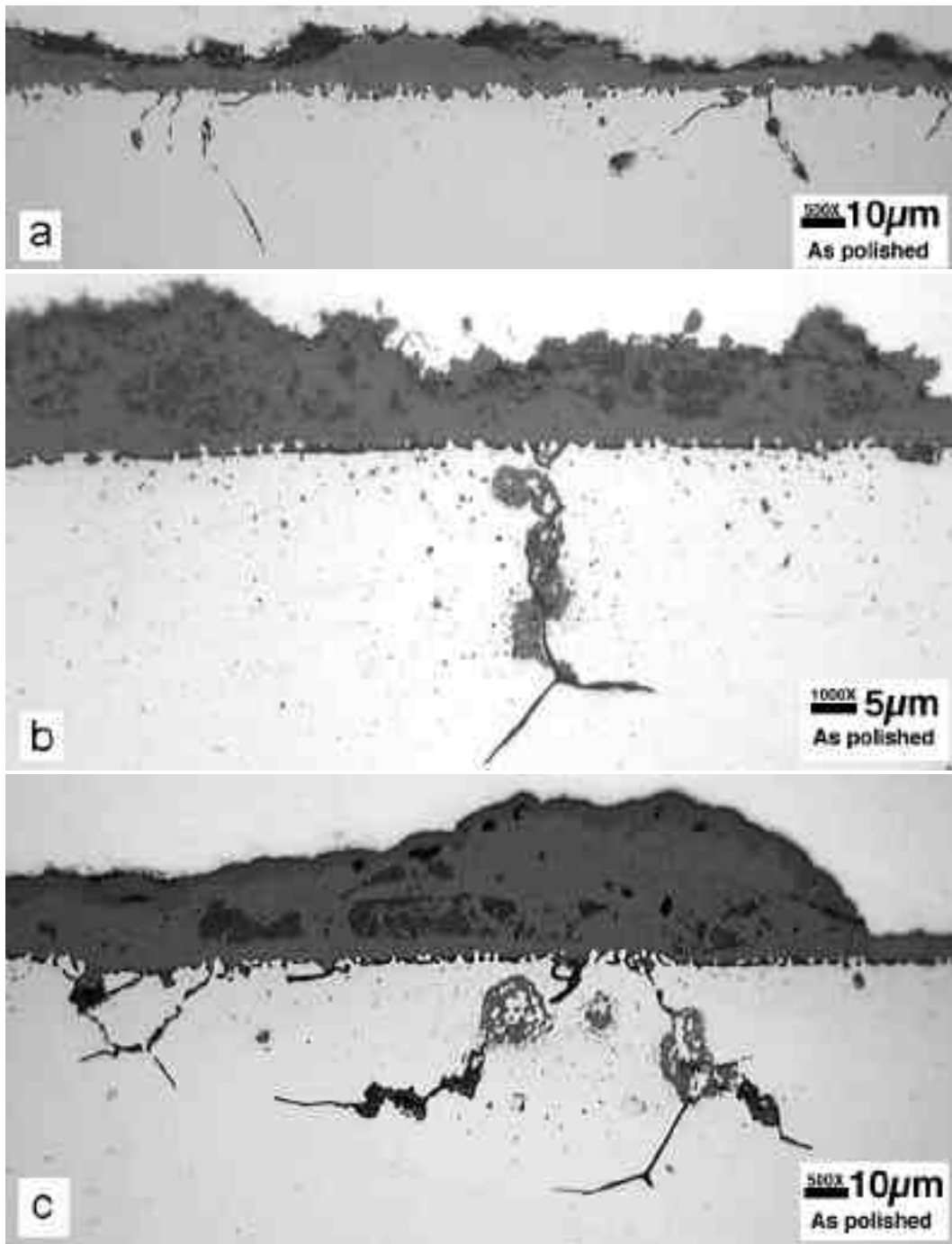


FIGURE 7 - Metallographic cross sections of alloy S31000 stainless steel after exposure in (a) air at 900°C for 500h; and (b and c) steam-10%CO₂ at 2 MPa and 900°C for 500h and 1000h, respectively.

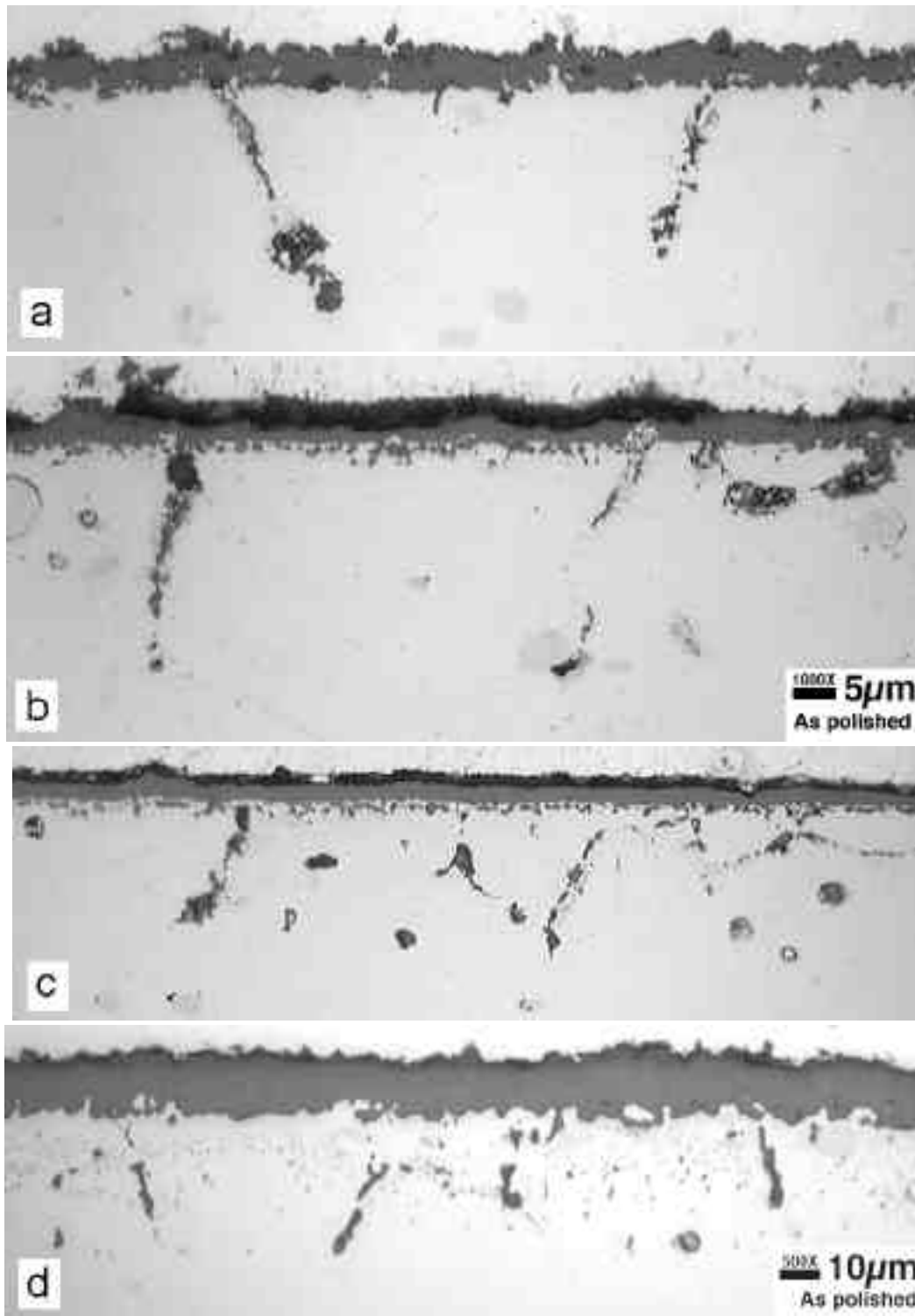


FIGURE 8 - Metallographic cross sections of alloy N06230 after exposure in (a) air at 900°C for 500h; (b and c) steam-10%CO₂ at 2 MPa and 900°C for 500h and 1000h, respectively; and (d) steam-10%CO₂ at 2 MPa and 1135°C for 740h. Figures a and b, and c and d, respectively, are at the same magnification.

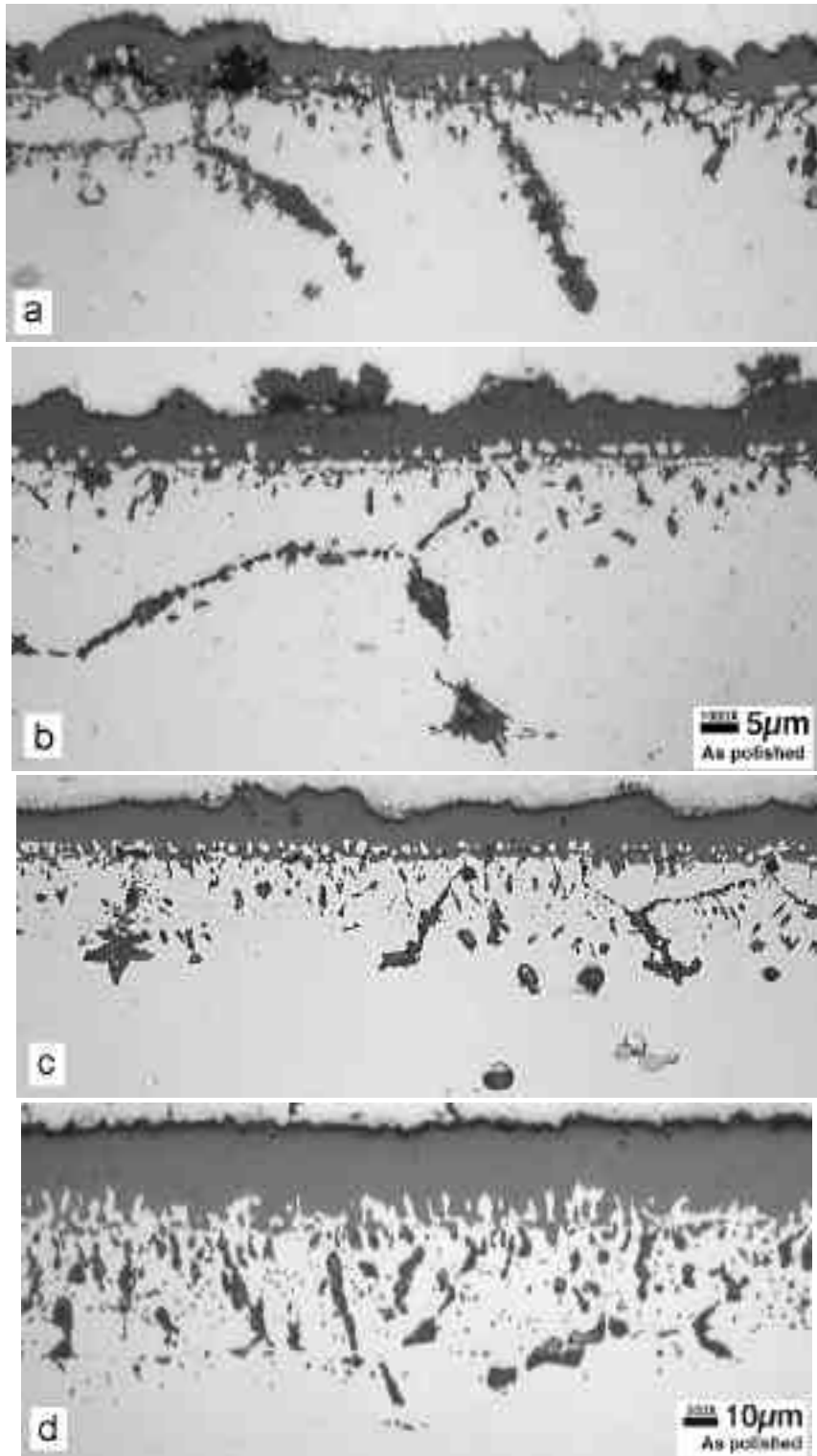


FIGURE 9 - Metallographic cross sections of alloy N06601 after exposure in (a) air at 900°C for 500h; (b and c) steam-10%CO₂ at 2 MPa and 900°C for 500h and 1000h, respectively; and (d) steam-10%CO₂ at 2 MPa and 1135°C for 740h.

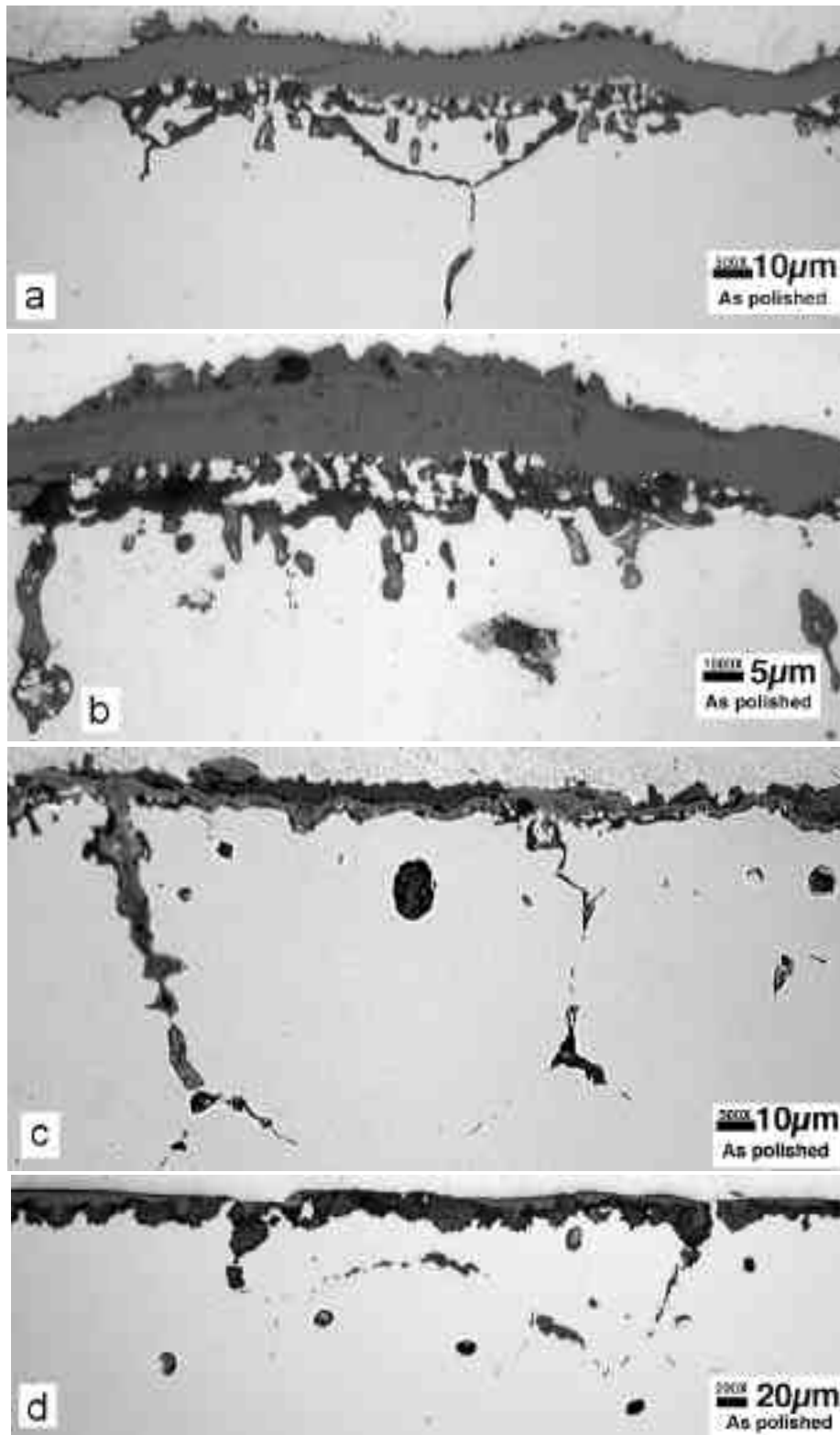


FIGURE 10 - Metallographic cross sections of alloy N12160 after exposure in (a) air at 900°C for 500h; (b and c) steam-10%CO₂ at 2 MPa and 900°C for 500h and 1000h, respectively; and (d) steam-10%CO₂ at 2 MPa and 1135°C for 740h.

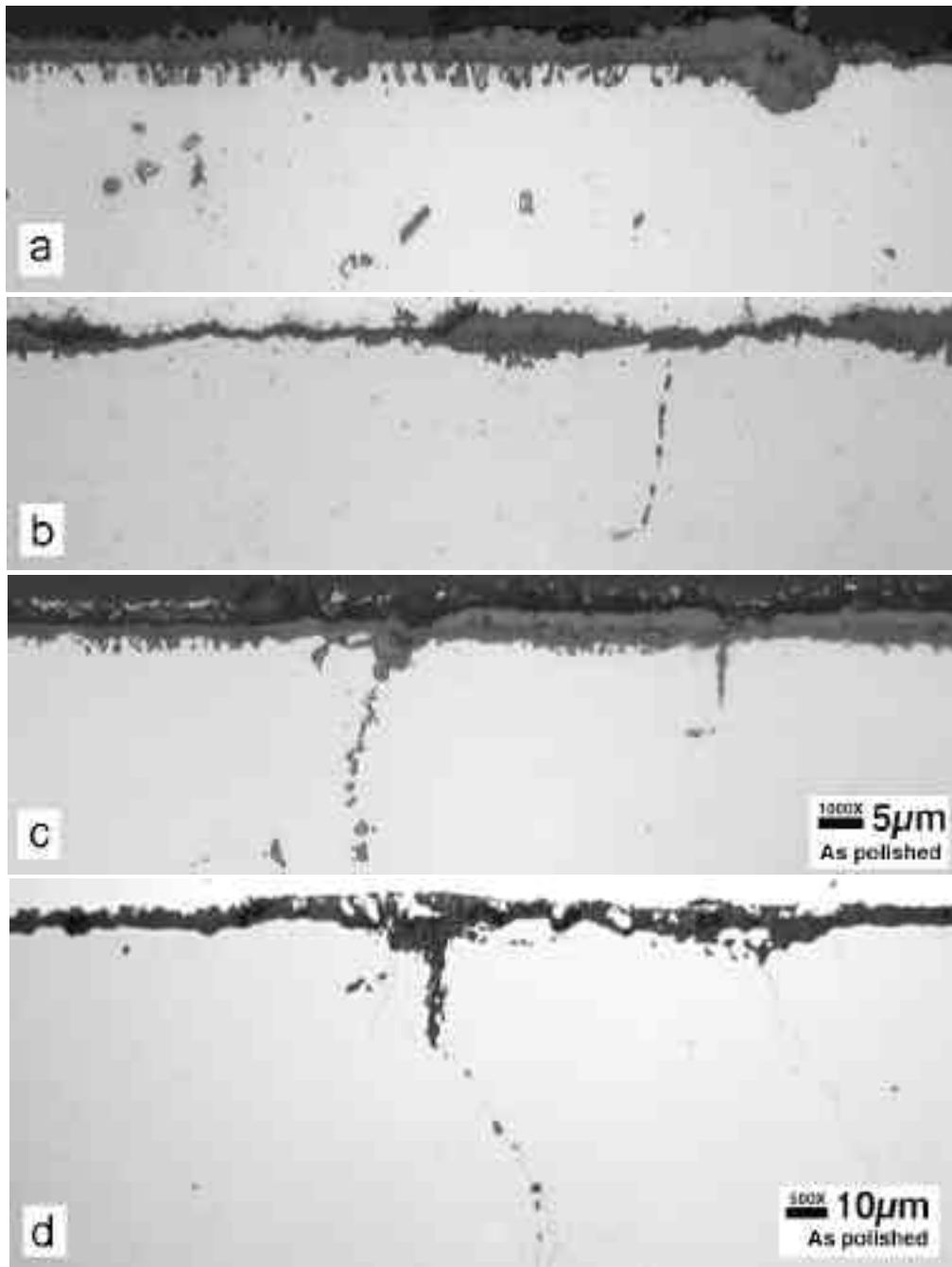


FIGURE 11 - Metallographic cross sections of alloy N07214 after exposure in (a) air at 900°C for 500h; (b and c) steam-10%CO₂ at 2 MPa and 900°C for 500h and 1000h, respectively; and (d) steam-10%CO₂ at 2 MPa and 1135°C for 740h.

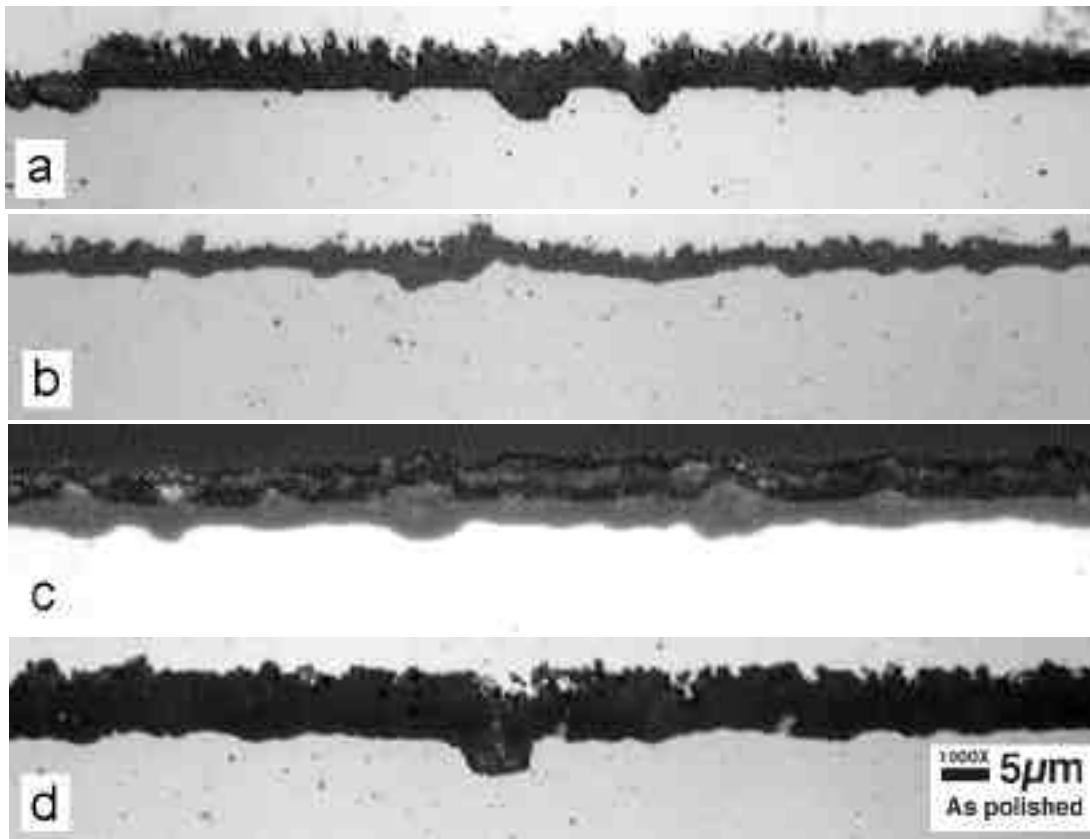


FIGURE 12 - Metallographic cross sections of alloy 956 after exposure in (a) air at 900°C for 500h; (b and c) steam-10%CO₂ at 2 MPa and 900°C for 500h and 1000h, respectively; and (d) steam-10%CO₂ at 2 MPa and 1135°C for 740h.